Available online at www.sciencedirect.com
ScienceDirect
Journal of Nuclear Materials 372 (2008) 285–292
journal of nuclear materials
www.elsevier.com/locate/jnucmat

Effect of heavy ion irradiation on microstructure of zirconium alloy characterised by X-ray diffraction

A. Sarkar, P. Mukherjee *, P. Barat

Variable Energy Cyclotron Centre, 1/AF Bidhannagar, Kolkata 700 064, India

Received 17 May 2006; accepted 2 March 2007

Abstract

Various X-ray diffraction line profile analysis (XRDLPA) techniques have been used to assess the microstructure of an heavy irradiated Zr–1.0%Nb–1.0%Sn–0.1%Fe alloy. The domain size, microstrain, density of dislocation and stacking fault probabilities of the irradiated alloy have been estimated as a function of dose by the Williamson–Hall Technique, a Modified Rietveld Analysis and by the Double Voigt Method. A clear signature for an increase in the density of dislocation with the dose of irradiation was revealed. The analysis also estimated the average density of dislocation in the major slip planes after irradiation.

PACS: 61.10.Nz; 61.72.−y; 61.82.Bg

1. Introduction

Energetic particles such as electrons, heavy ions and neutrons transfer energy to solid materials primarily by the process of ionization, electronic excitation and by the displacements of atoms from their original sites [1]. These processes cause a change in the internal microstructure, phase distributions, dimensions and the mechanical properties [2–5] of the target material. Generally neutrons and heavy ions in the MeV range impart so much energy to the primary knock-on that a displacement cascade is produced consisting of highly localized interstitials and vacancies [6] associated with a single initiating event. The process and the reaction pathways by which the displacement and electronic energy are dissipated, determine the structure and properties changes, exhibited by the material. Microstructural evolution in metals and alloys during irradiation with the energetic particles has been reviewed thoroughly with an emphasis placed on the underlying defect reaction processes [7]. In case of the light ions such as protons, the damage profiles are much more homogeneous than for heavy ions. The damage caused by the neutron irradiation is often simulated by using the high-energy particle irradiations, which allow easy variations of the irradiation conditions [6]. By using light or heavy ions, the recoil spectrum can be altered to cover significant ranges of the neutron recoil spectrum [6]. Thus the nature of the radiation damage in a material is affected by the type of ions used for irradiation, the alloying elements and the impurity variations [8].

In the present study, we have carried out irradiation with 145 MeV Ne^{6+} with degrader on Zr–1.0%Nb–1.0% Sn–0.1%Fe at different doses. Several techniques of X-ray diffraction line profile analysis (XRDLPA) have been used to evaluate the effect of the irradiation on the microstructure of the material. XRDLPA is a powerful technique to evaluate the microstructural parameters in a statistical manner [9]. Different techniques of XRDLPA have been widely applied for the evaluation of microstructural parameters in deformed metals and alloy systems [10,11]. In our earlier studies, we have measured microstructural

* Corresponding author. Tel.: +91 33 23371230; fax: +91 33 23346871.
E-mail address: paramita@veccal.ernet.in (P. Mukherjee).

0022-3115/$ - see front matter © 2007 Elsevier B.V. All rights reserved.
doi:10.1016/j.jnucmat.2007.03.217

variation due to irradiation with the proton and the oxygen ions on the same alloy [12,13]. Though the parameters obtained by different techniques are differently defined and thus not necessarily comparable, the main purpose of using these different techniques is to show their equivalence.

In this work, we have characterized the microstructural parameters by XRDLPA using three different model based approaches: (1) the Williamson–Hall Technique, (2) a Modified Rietveld Analysis and (3) a Double Voigt Method. The Zr–1.0%Nb–1.0%Sn–0.1%Fe alloy was irradiated with neon. The domain size, microstrain, density of dislocation and the stacking fault probabilities of the irradiated alloy have been estimated as a function of dose. The damage profile as a function of depth from the surface has been characterized in terms of displacements per atom (dpa) for different doses.

2. Experimental

An ingot of Zr–1.0%Nb–1.0%Sn–0.1%Fe alloy was prepared in the Nuclear Fuel Complex, Hyderabad, India, by the double vacuum arc melting technique. It was then β quenched, followed by hot extrusion and cold pilgering to produce fuel cladding tubes of 0.4 mm wall thickness.

Samples of size 10 mm × 10 mm were cut from these tubes and annealed at 1023 K for 4 h. The samples were mounted on an aluminum flange and covered with an aluminum foil of thickness 30 μm which was used as a degrader. These samples were then irradiated with 145 MeV Ne^{6+}ions from variable energy cyclotron (VEC), Kolkata, India. The incident energy of the particle on the sample was 110 MeV after degradation. The irradiation doses were 3×10^{17}, 8×10^{17}, 1×10^{18} and $3\times10^{18}Ne^{6+}$ ions/m^2. The flange used for irradiation was cooled by continuous flow of water. During the irradiation, the temperature of the sample did not rise above 313 K as measured by the thermocouple connected very close to the sample. The range of ions in this material and the dpa were obtained by Monte-Carlo simulation technique using the code SRIM 2000 [14].

X-Ray diffraction (XRD) profiles for each irradiated sample have been recorded from PHILIPS 1710 diffractometer using CuK_α radiation. The range of 2θ was from 25° to 100° and a step scan of 0.02° was used. The time per step was 4 s.

3. Method of analysis

In most X-ray investigations, structural information is extracted from the angular positions and the intensities of Bragg peaks in the diffraction pattern. Here, we are interested in variation of the microstructure with irradiation. Generally, the broadening of a Bragg peak arises due to the instrumental broadening, broadening due to the small domain size and microstrain. In general, more detailed information is extractable from the line shapes of the Bragg peaks; analysis of the line shapes allows for characterization of the microstructure more comprehensively in terms of the mean square microstrain and the average domain size. The Williamson–Hall Technique, a Modified Rietveld Method using the whole powder pattern fitting technique and a Double Voigt Analysis have been adopted in the present study in order to analyze the line shapes of the diffraction data of Zr–1.0%Nb–1.0%Sn–0.1%Fe at different doses of irradiation. The instrumental broadening correction was made using a standard defect free Si sample.

3.1. Williamson–Hall technique

Williamson and Hall [15] assumed that both size and the strain broadened profiles are Lorentzian. Based on this assumption, a mathematical relation was established between integral breadth (β), volume weighted average domain size (D_v) and the upper value of the microstrain (ε) as follows:

$$\frac{\beta\cos\theta}{\lambda}=\frac{1}{D_v}+2\varepsilon\left(\frac{2\sin\theta}{\lambda}\right). \tag{1}$$

The plot of $\left(\frac{\beta\cos\theta}{\lambda}\right)$ versus $S=\left(\frac{2\sin\theta}{\lambda}\right)$ gives the value of the microstrain from the slope and the domain size from the ordinate intercept.

3.2. Modified Rietveld method

In this method, the diffraction profiles have been modeled by pseudo-Voigt (pV) functions using the program LS1 [16].

This program refines simultaneously the lattice parameters, surface weighted average domain size (D_s), average microstrain $\langle\varepsilon_L^2\rangle^{\frac{1}{2}}$ and the preferred orientation parameter P [17,18] assuming isotropicity in the domain size and the microstrain. The effective domain size (D_e) with respect to each fault-affected crystallographic plane was refined to obtain the best fitting parameters.

XRD peak profiles of Zr–1.0%Nb–1.0%Sn–0.1%Fe show strong crystallographic texture along certain crystallographic directions particularly (0 0 2), (1 0 1), (1 0 2) and (1 0 3). The h,k,l values of these planes were incorporated in the program as the preferred oriented planes and the best fit was sought in each case.

Considering the X-ray line profiles to be symmetric in shape, distributions of the dislocations were assumed to be random. The average density of dislocation (ρ) has been estimated from the relation [19] $\rho=(\rho_D\rho_S)^{\frac{1}{2}}$, where, $\rho_D=\frac{3}{D_s^2}$ (density of dislocation due to domain) and $\rho_S=k\langle\varepsilon_L^2\rangle/b^2$ (density of dislocation due to strain), k is the material constant and b is the modulus of the Burger's vector, $\frac{1}{3}[1\,1\,\bar{2}\,0]$. Similarly, ρ_e, the density of dislocation at each crystallographic plane has been estimated.

D_e and D_s are related to the deformation stacking fault probability α, considering the growth fault probability (β) to be zero in the hcp alloys [20–24]. The values of α for various doses are reported.

3.3. Double Voigt technique

In this technique, the size and the strain effects are approximated by a Voigt function [25], which is a convolution of Gaussian and Cauchy functions. The equivalent analytical expressions for the Warren-Averbach size–strain separation [26] were then obtained. The Fourier coefficients $F(L)$ in terms of a distance, L, perpendicular to the diffracting planes is obtained by Fourier transform of the Voigt function [25] and can be written as:

$$F(L) = (-2L\beta_C - \pi L^2\beta_G^2), \tag{2}$$

where, β_C and β_G are the Cauchy and Gauss components of the total integral breadth, respectively.

β_C and β_G can be written as:

$$\beta_C = \beta_{SC} + \beta_{DC}, \tag{3}$$

$$\beta_G^2 = \beta_{SG}^2 + \beta_{DG}^2, \tag{4}$$

where, β_{SC} and β_{DC} are the Cauchy components of the size and the strain integral breadth, respectively, and β_{SG} and β_{DG} are the corresponding Gaussian components.

The size and the distortion coefficients were obtained considering at least two reflections from the same family of crystallographic planes. The surface weighted average domain size D_s and the microstrain $\langle\varepsilon_L^2\rangle^{\frac{1}{2}}$ are given by the equations:

$$D_s = 1/2\beta_{SC}, \tag{5}$$

$$\langle\varepsilon_L^2\rangle = [\beta_{DG}^2/(2\pi) + \beta_{DC}/(\pi^2 L)]/S^2,$$

$$\text{where } S = \frac{2\sin\theta}{\lambda}. \tag{6}$$

The volume weighted domain size [27] is given by $D_v = \frac{1}{\beta_S}$ where $\beta_S = \frac{\beta\cos\theta}{\lambda}$, integral breadth in the units of S, $(\text{Å})^{-1}$.

The surface weighted and the volume weighted column-length distribution functions are given by:

$$P_s(L) \propto \frac{d^2A_S(L)}{dL^2}, \tag{7}$$

$$P_v(L) \propto L\frac{d^2A_S(L)}{dL^2}. \tag{8}$$

For a size-broadened profile, the size coefficient is given as:

$$A_S(L) = \exp(-2L\beta_{SC} - \pi L^2\beta_{SG}^2). \tag{9}$$

From Eq. (8), we get,

$$\frac{d^2A_S(L)}{dL^2} = [(2\pi L\beta_{SG}^2 + 2\beta_{SC})^2 - 2\pi\beta_{SG}^2]A_S(L). \tag{10}$$

Selivanov and Smislov [28] showed that Eq. (9) is a satisfactory approximation of the surface weighted column-length distribution function.

4. Results and discussion

The range of 110 MeV Ne^{6+} ion in Zr–1.0%Nb–1.0%Sn–0.1%Fe (obtained by SRIM 2000 calculation) was found to be around 39 μm which is of the order of the depth of penetration of CuK_α X-ray in this material. The radiation damage was assayed by the damage energy deposited causing displacements of atoms. The total target displacements of the collision events calculated by the SRIM 2000 code is shown in Fig. 1. The damage is measured by the dpa. The average dpa for the highest dose sample in Zr–1.0%Nb–1.0%Sn–0.1%Fe was found to be 1.2×10^{-2}. The average dpa value has been calculated over the total range of 39 μm. The dpa value at 39 μm is found to be 0.13.

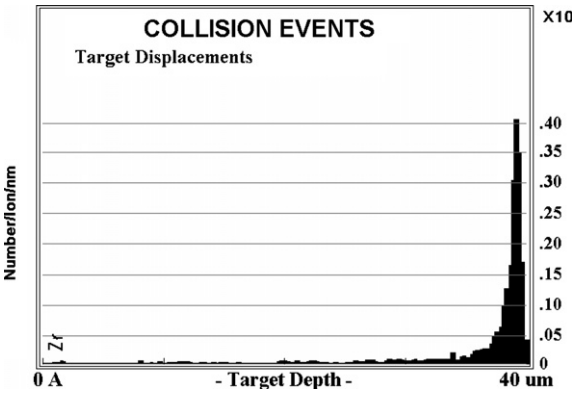

Fig. 1. Damage profile of 110 MeV Ne^{6+} in Zr–1.0%Nb–1.0%Sn–0.1%Fe.

4.1. Williamson–Hall technique

The Williamson–Hall (WH) technique estimates D_v and ε from the plot of $\left(\frac{\beta\cos\theta}{\lambda}\right)$ against $S = \frac{2\sin\theta}{\lambda}$. Fig. 2 shows the WH plots for the unirradiated and the irradiated Zr–1.0%Nb–1.0%Sn–0.1%Fe at different doses. For most of the cases, it is seen that $\frac{\beta\cos\theta}{\lambda}$ shows a linear S dependence. This implies that the shape of the domains is isotropic. It is further observed that the line connecting two orders of $(00l)$ type reflections, i.e. $\langle002\rangle$ and $\langle004\rangle$ yield a considerable slope indicating strong lattice distortion along $\langle001\rangle$ direction. The values of D_v and ε obtained from the

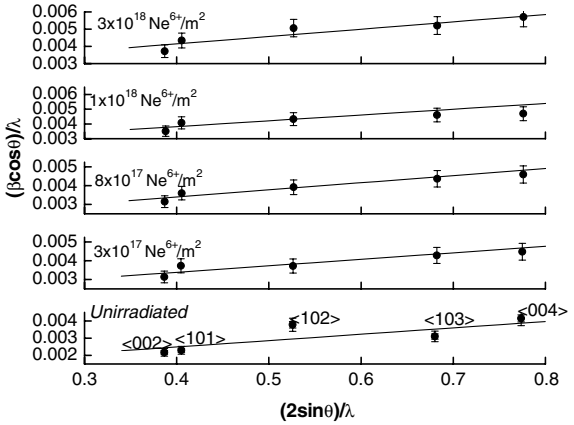

Fig. 2. Williamson–Hall plots for the unirradiated and irradiated Zr–1.0%Nb–1.0%Sn–0.1%Fe at different doses.

Table 1
Results of Williamson–Hall plot

Sample	Dose	Volume weighted average domain size (D_v) (nm) (±10%)	Microstrain (ε) (10^{-3}) (±5%)
Zirlo	Unirradiated	100.0	1.8
	3×10^{17} Ne^{6+}/m^2	50.0	1.8
	8×10^{17} Ne^{6+}/m^2	51.2	1.9
	1×10^{18} Ne^{6+}/m^2	45.4	2.0
	3×10^{18} Ne^{6+}/m^2	38.5	2.2

intercept and the slope of WH plots are shown in Table 1. It is observed that D_v decreased by a considerable amount in the first dose of irradiation. The values were found to decrease further with the dose. The value of ε was found to increase slightly with the dose.

4.2. Modified Rietveld method

We have carried out analysis on the XRD patterns of irradiated Zr–1.0%Nb–1.0%Sn–0.1%Fe with the help of modified Rietveld method using program LS1 [16]. The variation of D_s, $\langle\varepsilon_L^2\rangle^{\frac{1}{2}}$ and ρ for these samples have been plotted as a function of dose in Figs. 3–5, respectively.

Significant changes were found in the values of D_s, $\langle\varepsilon_L^2\rangle^{\frac{1}{2}}$ and ρ as a function of dose. The values of D_s initially decreased with increasing dose of irradiation but it saturated at higher dose. On the contrary, the average microstrain initially increased with dose of irradiation and consequently saturated at higher dose. The density of dislocation increased significantly for the irradiated samples and the increase was found to be almost an order of magnitude more for the case of the irradiated sample at a dose of 1×10^{18} Ne^{6+}/m^2 as compared to the unirradiated one. The density of dislocation was also found to saturate with dose.

The reason of the above findings can be explained as follows.

The range of 110 MeV Neon in Zr–1.0%Nb–1.0%Sn–0.1%Fe was found to be 39 μm as calculated by SRIM 2000. Neon being a heavy ion, transferred sufficient energy

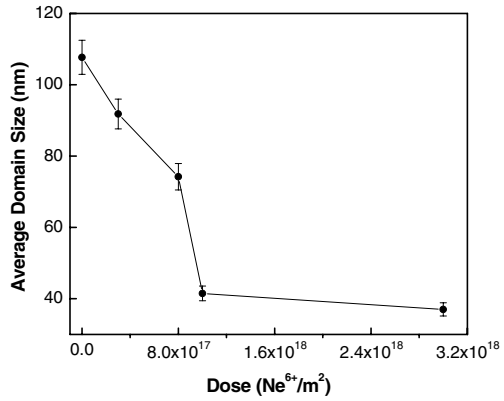

Fig. 3. Variation of average domain size as function of dose.

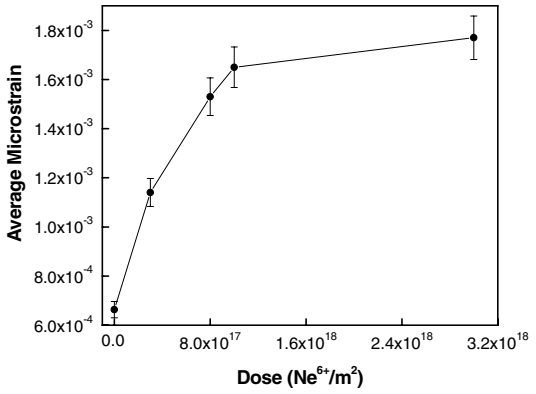

Fig. 4. Variation of average microstrain as function of dose.

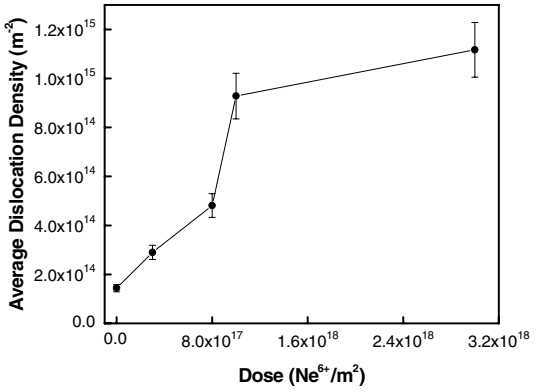

Fig. 5. Variation of average density of dislocation as function of dose.

to the primary knock-on atoms and a displacement cascade was produced consisting of highly localized interstitials and vacancies associated with a single initiated event. Moreover, the energy transferred to the lattice atoms was much larger at the end of the trajectory; as the primary recoil proceeded through the sample, losing energy in successive collisions, the displacement cross-section increased [29]. Thus the distance between the successive displacements decreased and at the end of the track, the recoil collided with practically every atom in its path, creating a very high localised concentration of the vacancies and the interstitials. These mobile point defects interact with the microstructure by long-range diffusion [6]. The main mechanism of the migration of the point migration and their annihilation are based on three reaction paths: (i) the loss of point defects at extended sinks such as the surfaces, grain boundaries and at the network of the existing dislocations, (ii) the nucleation of the clusters by the homogeneous reactions between the point defects of the same type, (iii) the growth of the defect clusters like the dislocation loops, and voids by agglomeration of the point defects.

For Ne^{6+} ion irradiation, the damage is maximum within a distance of 2–3 μm at the end of the reaction path, where the dpa is 0.13. A concentration gradient of defects in the sample was thus created within a small reaction path of 39 μm which helped in the migration of defects. Again,

the diffusion coefficient D_a of a particular lattice atom is enhanced due to irradiation [30] and is given by the following equation:

$$D_a = f_v D_v C_v + f_{2v} D_{2v} C_{2v} + f_i D_i C_i + \cdots\cdots \quad (11)$$

Thus, D_a is increased by increasing the concentration of different defect species such as the vacancies, di-vacancies, interstitials, etc., and also by opening up the other diffusion channels via defect species which are not significantly present in the normal thermally activated diffusion.

In the irradiated sample, the enhancement of radiation induced diffusion is solely responsible for the migration of the vacancies, their agglomeration and the collapsing in the shape of dislocation loops. This is the only mechanism by which density of dislocation is increased in the irradiated samples as Frank–Reed source mechanism for the multiplication of dislocation is absent due to the non-availability of any stress field. The generation of dislocation by collapsing of vacancy clusters is only possible when there is vacancy concentration in excess of the equilibrium values. Hence, we could observe an order of magnitude increase in the density of dislocation at a dose of 1×10^{18} Ne^{6+}/m^2. During irradiation, two competing processes occur simultaneously, one is the generation of vacancies, agglomeration of vacancies and then collapsing into dislocation loops and the other is, their annihilation at the possible sinks. Initially, at the low dose of irradiation (3×10^{17} Ne^{6+}/m^2), the rate of generation of dislocation loops dominates over the rate of annihilation of the point defects as the sink density is low. We therefore found an increase in the density of dislocation with dose. With increasing dose of irradiation, though more vacancies are created and the annihilation rate of vacancies also increases with sink density. Hence, a saturation was observed in the density of dislocation with the increase in the dose of irradiation.

The size of the domains of the irradiated samples decreased with the increase in the dose of irradiation. The decrease was quite drastic at lower doses and almost saturated at higher doses, as the generation of dislocations did not vary significantly at higher doses.

The effective domain size D_e, along different crystallographic directions were also found to decrease with dose as compared to the unirradiated material but the shape of the domains were almost isotropic. We have plotted the projections of D_e (along different directions) on the plane containing the directions $\langle 002 \rangle$ and $\langle 100 \rangle$. Only the projections in the first quadrant are shown in Fig. 6 for unirradiated and irradiated Zr–1.0%Nb–1.0%Sn–0.1%Fe. It was

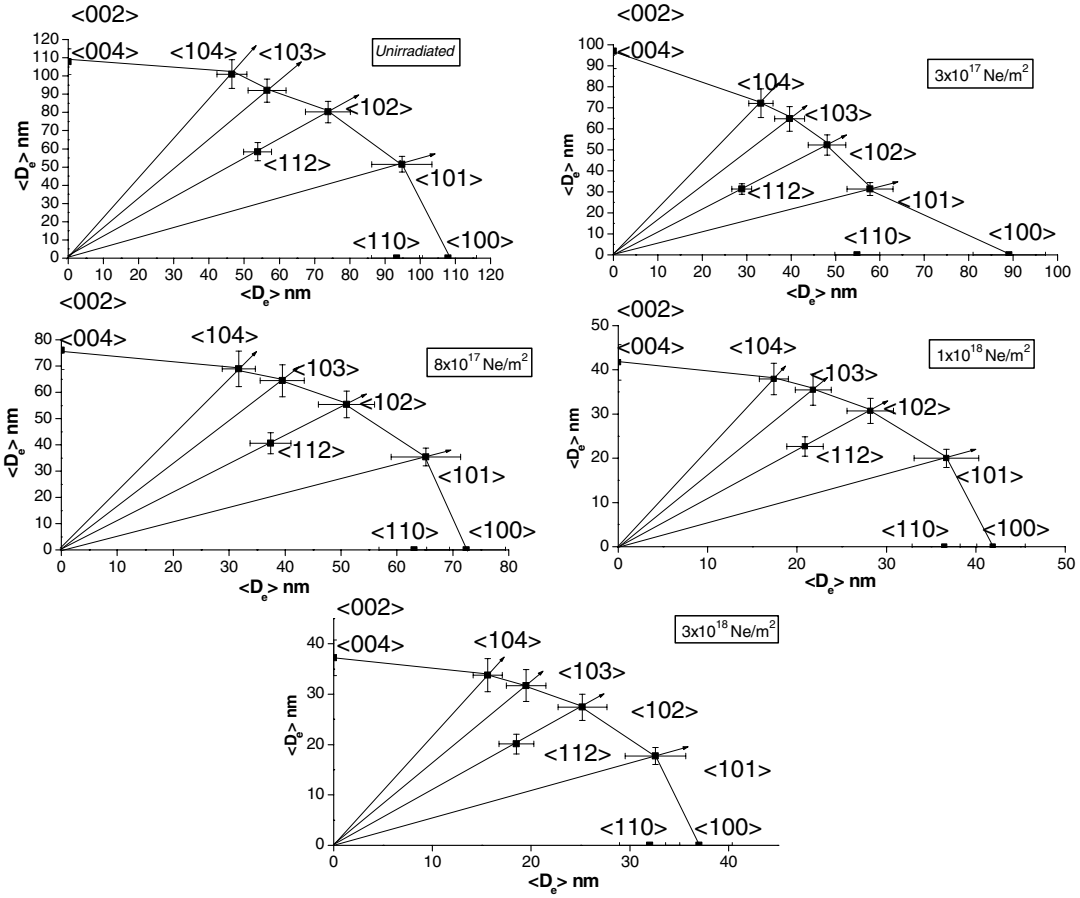

Fig. 6. Projections of effective domain size on the plane containing the directions $\langle 002 \rangle$ and $\langle 100 \rangle$ (First quadrant) for unirradiated and irradiated Zr–1.0%Nb–1.0%Sn–0.1%Fe at different doses.

clearly observed that D_e was almost isotropic (spherical) with values $\langle D_e\rangle_{002} \cong 1077$ Å and $\langle D_e\rangle_{100} \cong 1070$ Å for the unirradiated sample, $\langle D_e\rangle_{002} \cong 969$ Å and $\langle D_e\rangle_{100} \cong 891$ Å at a dose of $3\times10^{17}Ne^{6+}/m^2$, $\langle D_e\rangle_{002} \cong 760$ Å and $\langle D_e\rangle_{100} \cong 724$ Å at a dose of 8×10^{17} Ne^{6+}/m^2, $\langle D_e\rangle_{002} \cong 417$ Å and $\langle D_e\rangle_{100} \cong 419$ Å at a dose of $1\times10^{18}Ne^{6+}/m^2$ and $\langle D_e\rangle_{002} = 372$ Å and $\langle D_e\rangle_{100} = 370$ Å at a dose of $3\times10^{18}Ne^{6+}/m^2$. These values clearly signify that the shape of the domains did not change with dose though the variations in the size of the domains were significant with the increasing dose as compared to the unirradiated sample.

This analysis also revealed that the density of dislocation at each crystallographic plane has increased as a function of dose, as shown in Table 2. The analysis is important as the estimated values of the density of dislocation on various planes particularly on the slip planes provide information about the flow property of any material. The flow stress of metals is proportional to the square root of the density of dislocation [31]. In order to predict the number and the nature of the active slip systems, it is therefore essential to know the density of dislocations per slip plane [32].

The microstrain values at $L = 50$ Å along different crystallographic directions for the alloy at different doses are shown in Table 2. The values showed an increasing trend for irradiated samples as compared to the unirradiated one.

The deformation fault (α) was found to be negligibly small for the unirradiated and the irradiated samples.

4.3. Double Voigt analysis

The general conclusions obtained from the simple WH plot can be further substantiated by a more detailed analysis. In this analysis, both the size and the strain broadened profiles were approximated by a Voigt function. The Cauchy and the Gaussian components (β_{SC}, β_{SG}, β_{DC} and β_{DG}) of the size and the strain broadened profiles were then separated along $\langle 0\,0\,1\rangle$ and listed in Table 3. From Table 3, it is observed that in general size broadened profiles had both Cauchy and Gaussian components of the integral breadths.

The volume weighted column-length distribution function $P_v(L)$ along $\langle 0\,0\,l\rangle$ normal to the diffraction plane $(0\,0\,l)$ has been shown in Fig. 7. It is clear that the column length distribution is much wider for the unirradiated sample and it is found to narrow down with the increasing dose of irradiation.

Using different model based approaches of XRDLPA techniques, the microstructure of the irradiated Zr–1.0%Nb–1.0%Sn–0.1%Fe at different doses have been characterized. All these techniques are based on the profile shape and the broadening of the diffraction peak. Among these techniques, the Williamson–Hall gives the information of volume weighted domain size in a qualitative manner. The major advantage of this technique is that it is a very simple technique to ascertain whether the material is having anisotropy and also to get qualitative information about size and strain effects in the material independently.

Table 2
Microstrain and density of dislocation for Zr–1.0%Nb–1.0%Sn–0.1%Fe at different doses

Sample	Dose (Ne^{6+}/m^2) →	Microstrain (10^{-3}) Max. error ±0.00005					Dislocation density (10^{15}) (m^{-2}) Max. error ±(6×10^{13})				
		Unirradiated	3×10^{17}	8×10^{17}	1×10^{18}	3×10^{18}	Unirradiated	3×10^{17}	8×10^{17}	1×10^{18}	3×10^{18}
Zr–1.0%Nb–1.0%Sn–0.1%Fe	*Fault un-affected*										
	002	0.6	1.4	1.5	1.1	1.6	0.1	0.3	0.5	0.6	1.0
	004	0.6	1.4	1.5	1.1	1.6	0.1	0.3	0.5	0.6	1.0
	100	0.7	2.3	2.6	1.9	2.1	0.2	0.6	0.9	1.0	1.3
	110	0.7	1.4	2.0	1.4	1.8	0.1	0.5	0.6	0.8	1.1
	112	0.7	1.0	1.7	1.2	1.7	0.2	0.4	0.5	0.7	1.0
	Fault affected										
	101	0.6	1.3	2.1	1.6	1.9	0.2	0.5	0.7	0.9	1.2
	102	0.7	1.2	1.8	1.3	1.7	0.1	0.4	0.6	0.7	1.0
	103	0.7	1.2	1.7	1.2	1.7	0.2	0.6	0.5	0.7	1.0
	104	0.7	1.2	1.6	1.2	1.6	0.1	0.4	0.5	0.7	1.0
		Stacking fault probability (α) (10^{-4})									
		−0.20	−12.4	0.09	0.05	0.03					

Table 3
Results of double Voigt method for Zr–1.0%Nb–1.0%Sn–0.1%Fe at different doses

Sample	Dose	β_{SC} (10^{-3})	β_{SG} (10^{-3})	β_{DC} (10^{-3})	β_{DG} (10^{-3})	D_S (nm)	ε (10^{-3})	D_V (nm)
Zirlo[0 0 1]	Unirradiated	0.03	0.11	0.05	0.10	60.9	0.52	72.3
	$3\times10^{17}Ne^{6+}/m^2$	0.98	1.60	0.0	–	37.6	–	43.8
	$8\times10^{17}Ne^{6+}/m^2$	0.0	2.49	0.76	–	32.1	1.16	40.2
	$1\times10^{18}Ne^{6+}/m^2$	0.57	2.26	0.59	–	31.6	1.46	37.8
	$3\times10^{18}Ne^{6+}/m^2$	0.40	2.93	0.77	–	25.7	1.82	31.4

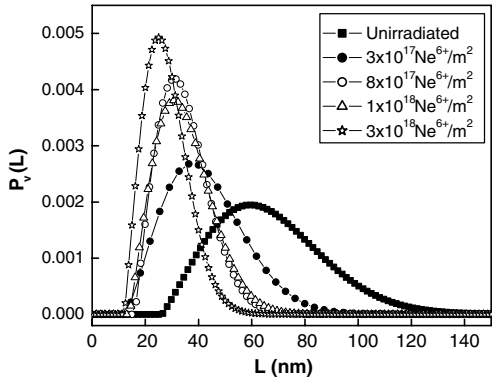

Fig. 7. Volume weighted column length distribution function for unirradiated and irradiated Zr–1.0%Nb–1.0%Sn–0.1%Fe at different doses.

Double Voigt method gives information about the microstructure considering only the parallel peaks. On the contrary the Modified Rietveld method gives quantitative information of the microstructural parameters considering all the diffraction peaks. These techniques have limitations in characterising the small defects particularly small interstitial clusters which do not cause broadening of the peak but contribute to the background values close to the Bragg peak [33]. Scattering of X-rays from interstitial clusters [34] contribute to diffuse scattering very close to the Bragg peak (Huang scattering). Thus, more complete information of the microstructure of the irradiated samples can be obtained from X-ray diffraction techniques by the combined studies of the diffraction pattern in the Bragg peak region (coherent scattering) and in the background region (diffuse scattering close to the Bragg peak). As in our case, the experiments were carried out at room temperature, the diffuse scattering near the Bragg peak region due to small interstitial clustering are superimposed by thermal diffusion scattering. Hence, the line profile analysis could characterise only those microstructural parameters which are responsible for the broadening of the diffraction peaks.

5. Conclusion

XRDLPA can be used as a technique to analyze change in the microstructure of materials due to radiation damage. In this work, the microstructure of the unirradiated and irradiated Zr–1.0%Nb–1.0%Sn–0.1%Fe has been assessed by XRDLPA using different model based approaches. Microstructural parameters like average and effective domain sizes and microstrain within the domains have been characterised as a function of dose. The density of dislocation and the stacking fault probability have been estimated from these values. The analysis reveals that there is a significant decrease of surface weighted average domain size (D_s) with dose. The damage associated with neon beams (a heavy ion) is quite extensive and produces highly localized concentrations of defects, particularly vacancies and interstitials. These vacancy clusters collapse into dislocation loops and the dislocation density increases accordingly. This analysis also estimated the average density of dislocation in the major slip planes. The deformation (stacking) fault probability was found to negligible for this alloy even with increasing dose of irradiation. The column length distribution was found to be narrower at highest dose of irradiation for this alloy.

References

[1] A. Seeger, in: Proceedings of 2nd UN International Conference on Peaceful Uses of Atomic Energy, Geneva, 1958, vol. 6, United Nations, New York, 1958, p. 250.
[2] M.J. Makin, T.H. Blewitt, Acta Metall. 10 (1962) 241.
[3] R. Higgy, F.H. Hammad, J. Nucl. Mater. 55 (1975) 177.
[4] G.S. Was, S.M. Bruemmer, J. Nucl. Mater. 216 (1994) 326.
[5] L.K. Mansur, J. Nucl. Mater. 216 (1994) 97.
[6] C. Abromeit, J. Nucl. Mater. 216 (1994) 78.
[7] M. Kiritani, J. Nucl. Mater. 216 (1994) 220.
[8] M. Griffiths, J. Nucl. Mater. 159 (1988) 190.
[9] P. Mukherjee et al., Acta Mater. 52 (2004) 5687.
[10] M. De, S.P. Sengupta, Pramana 23 (1984) 721.
[11] J.B. Cohen, C.N.J. Wagner, J. Appl. Phys. 33 (1962) 2073.
[12] P. Mukherjee et al., J. Nucl. Mater. 297 (2001) 341.
[13] P. Mukherjee et al., J. Nucl. Mater. 305 (2002) 169.
[14] J.P. Biersack, L.G. Haggmark, Nucl. Instrum. and Meth. 174 (1980) 257, The Stopping and Range of Ions in Matter (SRIM 2000) software developed by J. Ziegler and J.P. Biersack is available on the Website http://www.research.ibm.com/ionbeams.
[15] G.K. Williamson, W.H. Hall, Acta Metall. 1 (1953) 22.
[16] L. Lutterotti, P. Scardi, J. Appl. Cryst. 23 (1990) 246.
[17] W.A. Dollase, J. Appl. Cryst. 19 (1986) 267.
[18] G. Will, M. Belloto, W. Parrish, M. Hatr, J. Appl. Cryst. 21 (1988) 182.
[19] G.K. Williamson, R.E. Smallman, Philos. Mag. 1 (1956) 34.
[20] B.E. Warren, X-ray Diffraction, Addision-Wesley, Reading (MA), 1969, p. 251.
[21] S.K. Chatterjee, S.K. Halder, S.P. Sengupta, J. Appl. Phys. 47 (1976) 411.
[22] S.K. Chatterjee, S.P. Sengupta, J. Mater. Sci. 9 (1974) 953.
[23] R. Sen, S.K. Chattopadhyay, S.K. Chatterjee, Jpn. J. Appl. Phys. 36 (1997) 364.
[24] R. Sen, S.K. Chattopadhyay, S.K. Chatterjee, Metall. Mater. Trans. A 29 (1998) 2639.

[25] D. Balzar, H. Ledbetter, J. Appl. Cryst. 26 (1993) 97.
[26] B.E. Warren, B.L. Averbach, J. Appl. Phys. 21 (1950) 595.
[27] P. Scherrer, Nachr Gott 2 (1918) 98.
[28] V.N. Selivanov, E.F. Smislov, Zavod Lab 57 (1991) 28.
[29] R.W. Weeks, R.O. Scattergood, S.R. Pati, J. Nucl. Mater. 36 (1970) 223.
[30] R. Sizmann, J. Nucl. Mater. 69&70 (1978) 386.
[31] S.J. Basinski, Z.S. Basinski, in: F.R.N. Nabarro (Ed.), Dislocations in Solids, vol. 4, North Holland, Amsterdam, 1979, p. 261.
[32] R. Madec, B. Devincre, L. Kubin, T. Hoc, D. Rodney, Science 301 (2003) 1879.
[33] J.B. Roberto, B. Schoenfeld, P. Ehrhart, Phys. Rev. B 18 (1978) 2591.
[34] P. Ehrhart, J. Nucl. Mater. 69&70 (1978) 200.